doi:10.1006/jmbi.2001.4749 available online at http://www.idealibrary.com on IDEAL® J. Mol. Biol. (2001) 309, 181–192

JMB

Binding Site Differences Revealed by Crystal Structures of *Plasmodium falciparum* and Bovine Acyl-CoA Binding Protein

D. M. F. van Aalten[1]*, K. G. Milne[1], J. Y. Zou[2], G. J. Kleywegt[2] T. Bergfors[2], M. A. J. Ferguson[1], J. Knudsen[3] and T. A. Jones[2]

[1]*Wellcome Trust Biocentre Department of Biochemistry University of Dundee, Dundee DD1 5EH, Scotland*

[2]*Department of Cell and Molecular Biology, Uppsala University, Biomedical Centre Box 596, SE-75124, Uppsala Sweden*

[3]*Institute of Biochemistry Odense University DK-5320, Odense, Denmark*

**Corresponding author*

Acyl-CoA binding protein (ACBP) maintains a pool of fatty acyl-CoA molecules in the cell and plays a role in fatty acid metabolism. The biochemical properties of *Plasmodium falciparum* ACBP are described together with the 2.0 Å resolution crystal structures of a *P. falciparum* ACBP-acyl-CoA complex and of bovine ACBP in two crystal forms. Overall, the bovine ACBP crystal structures are similar to the NMR structures published previously; however, the bovine and parasite ACBP structures are less similar. The parasite ACBP is shown to have a different ligand-binding pocket, leading to an acyl-CoA binding specificity different from that of bovine ACBP. Several non-conservative differences in residues that interact with the ligand were identified between the mammalian and parasite ACBPs. These, together with measured binding-specificity differences, suggest that there is a potential for the design of molecules that might selectively block the acyl-CoA binding site.

Keywords: acyl-CoA; structure; *Plasmodium falciparum*; drug design; X-ray crystallography

Introduction

Human malaria is caused by the protozoan parasite *Plasmodium falciparum*. Although drugs are available, there is an increasing demand for new pharmaceuticals due to the emergence of drug-resistant parasites.[1] The increasing wealth of sequence data from both the *P. falciparum* and the human genome projects, in combination with structural data, facilitate the design of novel drug leads on a rational basis. Here, we describe the crystal structures of bovine and *P. falciparum* acyl-CoA binding protein, characterize differences between the ligand-binding sites and assess the potential for exploitation of these differences in the design of blocker molecules selective for the *P. falciparum* protein.

Acyl-coenzyme A binding proteins (ACBPs) are a family of 86 to 103 residue proteins with conserved amino acid sequences.[2] A total of 30 sequences have been described from a wide range of species and genomic sequence data, such as from *Caenorhabditis elegans*, have suggested the existence of other proteins that contain ACBP-like domains.[3] Long chain acyl-CoA esters serve as important intermediates in lipid synthesis and fatty acid degradation. Besides this house-keeping function, a large body of evidence has accumulated indicating that long-chain acyl-CoA esters also have an important function in the regulation of intermediary metabolism and gene regulation.[2,4] In *Trypanosoma brucei*, ACBP has been shown to be an important component in glycosylphosphatidylinositol (GPI) biosynthesis,[5] donating myristoyl-CoA for the fatty acid remodelling reactions.[6] ACBPs typically bind saturated and unsaturated C_{14}-C_{22} acyl-CoA esters with 1:1 stoichiometry and a high degree of affinity ($K_d = 2$-10 nM).[2] Long-chain acyl-CoA esters are amphipathic molecules which can partition into phospholipid bilayers and inhibit a large number of cellular functions and enzymes

Abbreviations used: ACBP, acyl-coenzyme A-binding protein; bACBP, bovine ACBP; CoA, coenzyme A; CC, correlation coefficient; GPI, glycosylphosphatidylinositol; NCS, non-crystallographic symmetry; ORF, open reading frame; PCR, polymerase chain reaction; PfACBP, ACBP from *Plasmodium falciparum*; RBR, rigid body refinement; RMSD, root mean square deviation; SA, simulated annealing.

E-mail address of the corresponding author: dava@davapc1.bioch.dundee.ac.uk

0022-2836/01/010181–12 $35.00/0

at low concentrations.[2] The function of long-chain acyl-CoA enzymes as intermediates in lipid metabolism and as regulators of cell signaling requires the maintenance of an acyl-CoA pool bound to a transporter protein for rapid deployment. The principal molecule in the eukaryotic cell that fulfills this role is ACBP. The sequences of expressed ACBPs contain a subset of highly conserved residues (Figure 1). This subset contains both polar and non-polar residues, distributed evenly through the sequence. Mutational studies have shown that several evolutionary conserved residues (e.g. Tyr31, Gln33, and Lys54) play key roles in the function, stability, and folding of ACBP.[7,8]

The three-dimensional structure of recombinant bovine ACBP and of ACBP complexed with palmitoyl-CoA has been determined by NMR.[9,10] It consists of four α-helices arranged in a bowl shape with a highly exposed acyl-CoA-binding site (Figure 2). The ligand is bound through specific interactions with residues on the protein, most notably several conserved positive charges that interact with the phosphate group on the adenosine-3′-phosphate moiety, and the acyl chain is sandwiched between the hydrophobic surfaces of CoA and the protein.

Here, the cloning, expression and characterization of ACBP from *P. falciparum* is described, together with the 2.0 Å crystal structures of *P. falciparum* and bovine ACBP (two crystal forms). The results are discussed with respect to the possibility of selective blocker design.

Results

Characterization of PfACBP

The *P. falciparum* ACBP (Pf ACBP) sequence was identified through a sequence search in the *P. falciparum* genome database, cloned and overexpressed in *Escherichia coli*. Mass spectrometry of the purified protein (data not shown) identified a 10,867 Da protein corresponding to PfACBP. The specificity of acyl-CoA binding to PfACBP and bovine ACBP (bACBP) was investigated by a competition binding assay and is compared in Figure 3(a). It appears that the ACBPs have a different preference in binding acyl-CoA: PfACBP has a weak optimum at $C_{14:0}$ and can also bind shorter-chain acyl-CoA enzymes, whereas bACBP prefers longer-chain acyl-CoA enzymes, centred around $C_{18:0}$. HPLC analysis of acyl-CoAs associated with purified recombinant PfACBP confirmed its slectivity for shorter-chain acyl-CoA species (Table 1). This preference of PfACBP for shorter chain lengths was further investigated using iso-electric focusing gels. Consistent with the previous data, PfACBP has a broad specificity for binding shorter chain acyl-CoAs (Figure 3(b)) whereas bACBP was unable to bind acyl-CoAs shorter than $C_{12\text{-}14:0}$ in this assay (Figure 3(c)).

Table 1. Acyl-CoA composition derived by HPLC on total acyl-CoA from recombinant PfABCP

C_{12}:0	15.2%
C_{14}:0	9.1%
C_{14}:1	9.1%
C_{16}:0	22.2%
C_{16}:1	21.5%
C_{18}:0	0.5%
C_{18}:1	6.5%
C_{18}:2	4.9%
Unknown compound I	10.8%
Unknown compound II	0.3%

Overall description of the structures

The structures of apo-bACBP (orthorhombic and tetragonal crystal forms) and PfACBP in complex with acyl-CoA were solved by molecular replacement (using the NMR structure and the apo-bACBP structure as a model, respectively) and refined to 2.0 Å resolution. All three structures have good stereochemistry (Table 2), with either one (Met46) or no residues in disallowed regions of the Ramachandran plot.[11] The backbone and most side-chains were well defined by the electron density maps (Figure 2), although some disorder was seen for a few solvent-exposed side-chains. There was evidence for alternate side-chain confor-

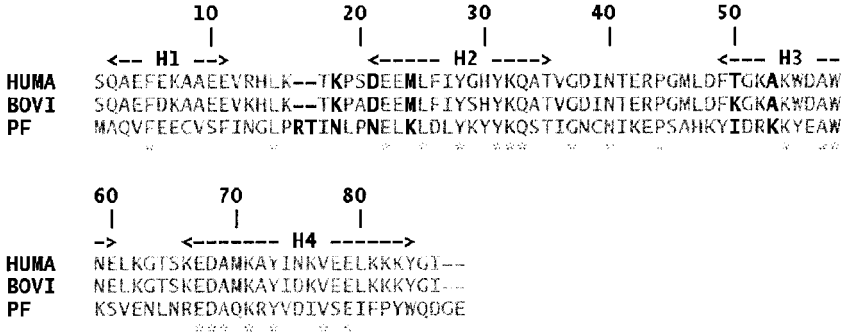

Figure 1. ACBP structure-based sequence alignment. Human (HUMA), bovine (BOVI) and *P. falciparum* (PFACBP) are aligned. The positions of the four α-helices are indicated (H1-4). Differences between bovine and *P. falciparum* ACBP are indicated in bold; conserved residues are marked by an asterisk. The bovine sequence numbering is used.

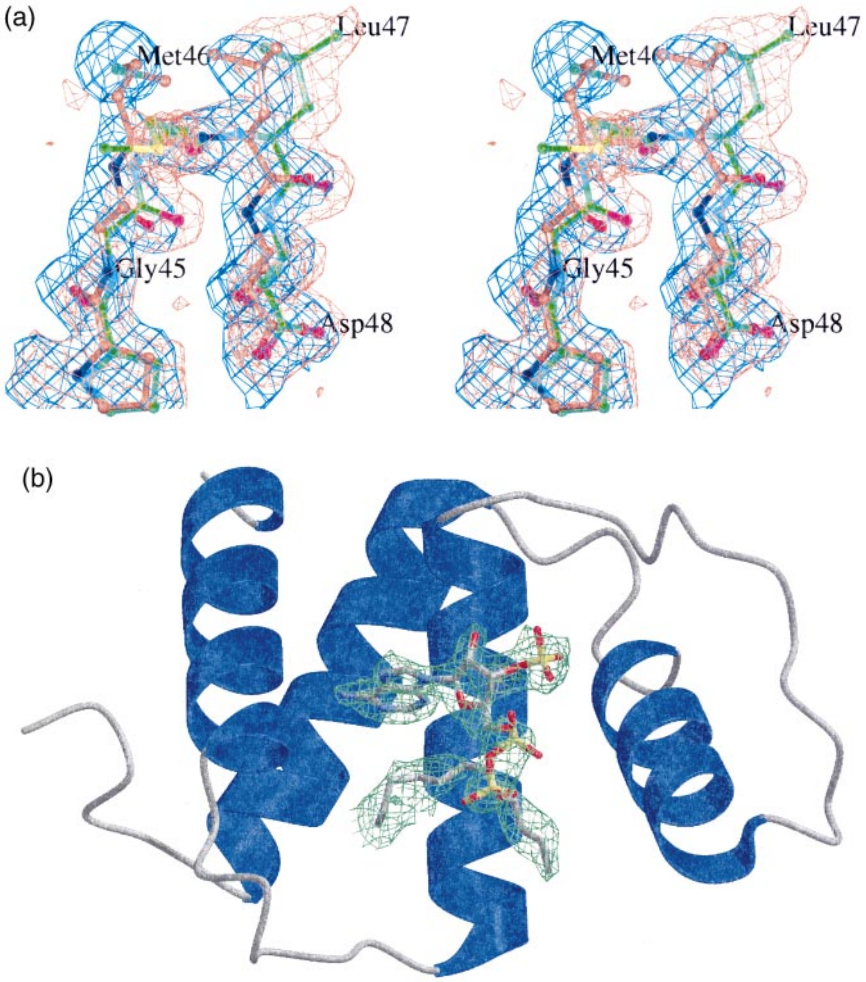

Figure 2. Overall structure and electron density maps. (a) Stereo image of bACBP in the tetragonal crystal form with carbon atoms coloured green, nitrogen atoms light blue and oxygen atoms mangenta. For ACBP in the orthorhombic crystal form, carbon atoms are shown in gold, nitrogen atoms in blue, and oxygen atoms in red. SigmaA weighted $2F_o - F_c$ maps are shown in blue (orthorhombic bACBP) and orange (tetragonal bACBP). (b) PfACBP, with backbone shown as blue ribbon. The acyl-CoA ligand is shown as a stick model. The $F_o - F_c$ maps just before inclusion of the adenosine-3′-phosphate and the fatty acid are shown at 2.5 and 2.0 σ, respectively (red).

mations, some of which were modelled in the PfACBP structure. No density was present for the two C-terminal PfACBP residues, which were therefore not modelled. The differences between PfACBP and bACBP (orthorhombic form) are significant with an RMSD value of 1.3 Å on all corresponding C^{α} atoms (see Table 3 and Figure 4(a)).

Although bACBP was co-crystallized with palmitoyl-CoA, no density was observed for the ligand. PfACBP was not co-crystallized with any added acyl-CoA, yet strong density for the adenosine-3′-phosphate and later the acyl chain was observed (Figure 2(b)). HPLC analysis confirmed the presence of a ligand (Table 1) and showed that it was a mixture of acyl-CoA species. Density at the end of the acyl chain was well defined, but from C2 onwards to the adenosine-3′-phosphate the density could not be interpreted unambiguously, and these atoms were not modelled. It is possible that the protein accomodated a mixture of acyl chain lengths by keeping CoA and the end of the acyl chain tethered, allowing the intermediate atoms to adopt different conformations. This is consistent with the HPLC analysis and the disorder observed in the crystal structure.

Comparison of the two bACBP crystal forms

The structures of bACBP in the two crystal forms are very similar. The three molecules in the tetragonal crystal form have RMSD values of 0.5(±0.2) Å on C^{α} atoms to the molecule in the orthorhombic crystal form (Table 3). The main difference is around the region Gly45 to Asp48. In the orthorhombic form, this region adopts a type I turn structure, while a type II′ turn is present in the tetragonal form. This causes the side-chain of Met46 to point into opposite directions in the two structures (Figure 2(a)). The electron density maps are clear for this part of the structure in both forms

Table 2. Refinement and model statistics

	Orthogonal-bACBP	Tetragonal-bACBP	PfACBP
Resolution range (Å)	19-2.0	19-2.0	20-2.0
Number of reflections	6394	18,784	7754
Number of test reflections	647	941	500
R	0.200	0.223	0.198
R_{free}	0.226	0.255	0.237
Number of atoms	699	2109	896
Number of water molecules	60	211	85
RMSD from ideal geometry[27]			
Bond lengths (Å)	0.005	0.006	0.0096
Bond angles (deg.)	0.8	0.9	1.5
B-factor RMSD bonds (main-chain, Å^2)	2.5	2.5	1.6
B-factor RMSD bonds (side-chain, Å^2)	2.5	2.5	2.3
Average *B*-factor (main-chain, Å^2)	22.6	22.2	30.9
Average *B*-factor (side-chain, Å^2)	27.4	24.5	33.0
Average *B*-factor (water, Å^2)	30.5	27.7	45.8
Average *B*-factor (other, Å^2)	51.5	19.4	50.0
RMSD difference C$^\alpha$ atoms (Å)	-	0.06	-
RMSD difference all atoms (Å)	-	0.4	-

All measured reflections were used for refinement. About 5 % of the data were randomly selected and excluded from the refinement and used for calculation of R_{free}.

(Figure 2(a)), although the side-chain atoms of Met46 in the tetragonal form show elevated temperature factors. The distances between corresponding C$^\alpha$ atoms in the two structures are 2.2 Å for Met46 and 1.0 Å for Leu47. This difference is most likely caused by different crystal packing environments. If Met46 in the tetragonal form had a similar conformation as in the orthorhombic form, it would have clashed with the side-chain of Met24 of an NCS-related molecule. The three molecules in the asymmetric unit of the tetragonal form adopt rather different conformations for the side-chain of Met46, although the main-chain conformations are almost identical. This might reflect the flexibility of Met46 side-chain atoms in solution. From Asp48 onwards, the two structures overlap again. Some polar side-chains have different conformations in the two crystal forms, partially caused by different hetero-entities present in the two crystals. For example, the binding of sulphate ions in the tetragonal form crystal affects the side-chain orientations of Lys50 and Lys54, and the binding of cadmium ions in the orthorhombic form affects the side-chain of Glu10 and Glu42. The other differences between the polar side-chains in the two crystal forms are probably due to the intrinsic flexibility of these residues, since their side-chains were associated with rather poor electron densities in one or both forms.

Comparisons of the bACBP NMR and crystal structures

The structures of bACBP have been determined by NMR in both apo form and in complex with palmitoyl-coenzyme A.[9,10] Since both our crystal forms contain bACBP in the apo form, the comparisons are performed with the apo form NMR structures (PDB entry 2ADB). There are 29 models available which all fit the experimental NMR data. For convenience, the central model in the cluster, which is defined as the model that has the smallest RMSD compared to all other models, was used for the comparisons with crystal structures. In 2ADB, model 17 has the lowest RMSD (0.62 Å using C$^\alpha$ atoms) to the rest of the models. All subsequent comparisons were done against this model. The three NCS-related molecules in the tetragonal form are similar (pair-wise RMSD after superposition on C$^\alpha$ atoms is less than 0.1 Å), so an arbitrarily chosen molecule (in this case molecule A) has been used for the comparisons. The overall molecular architecture of the NMR and crystal structures of bACBP is very similar, as shown in Figure 4(a), although there are some large local differences,

Table 3. Comparison of the ACBP backbones

	PfACBP	bACBP_o	bACBP_t	bACBP_NMR
PfACBP		1.3	1.3	1.9
bACBP_o			0.5	1.9
bACBP_t				1.9

Structures were pairwise superposed and RMSD values on C$^\alpha$ atoms were calculated, listed in Å in the Table. The loop carrying the extra two amino acids in PfACBP (Figure 1) and the six C-terminal amino acids were not included in the comparisons. bACBP_o, bovine ACBP in the orthorhombic crystal form, bACBP_t, bovine ACBP in the tetragonal crystal form; bACBP_NMR, bovine ACBP NMR structure (17th model from PDB entry 2ADB).

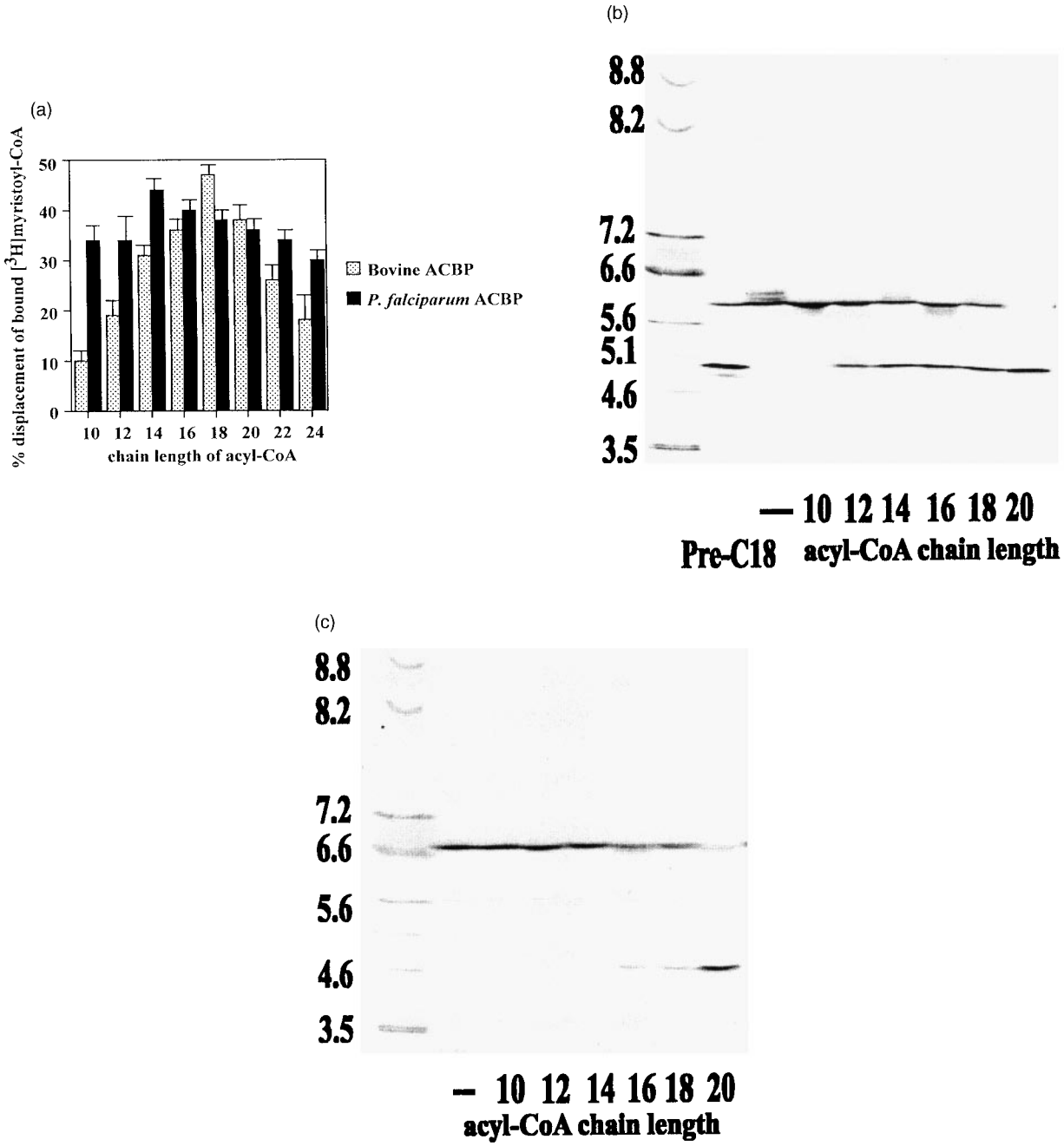

Figure 3. (a) Relative specificities of PfACBP and bACBP for acyl-CoA chain length measured by the lipidex assay. PfACBP and bACBP were incubated with [^{3}H]myristoyl-CoA in the presence or absence of acyl-CoAs of various chain lengths as indicated. The percentage of [^{3}H]myristoyl-CoA displaced from ACBP by the different unlabelled acyl-CoAs is shown as the mean (±S.E.) ($n = 3$). (b) Isoelectrofocusing of purified recombinant PfACBP prior to stripping bound acyl-CoAs by C18-reverse phase HPLC (lane 2). PfACBP was incubated in the absence or presence of acyl-CoAs as indicated. (c) Isoelectrofocusing of bACBP in the absence or presence of acyl-CoAs as indicated.

especially in the loops connecting the helices. The RMSD on C^α atoms between the NMR structure and the crystal structures in orthorhombic and tetragonal forms is 1.9 Å for both superpositions (Table 3). Figure 4(b) shows the distance between the corresponding C^α atoms of the NMR and crystal structures of bACBP as a function of residue number. An accurate torsion angle difference plot requires that the individual atoms of the peptide group be well defined,[12] which is not always achieved with the NMR models. Instead a plot of the differences of the dihedral angles of sequential C^α atoms between the crystal and NMR structures is more appropriate (Figure 4(c)). This plot is, of course, considerably less noisy than the equivalent plot based on differences of ϕ and ψ angles. It is clear from the plot that the helical parts of the structures are more similar than the connecting

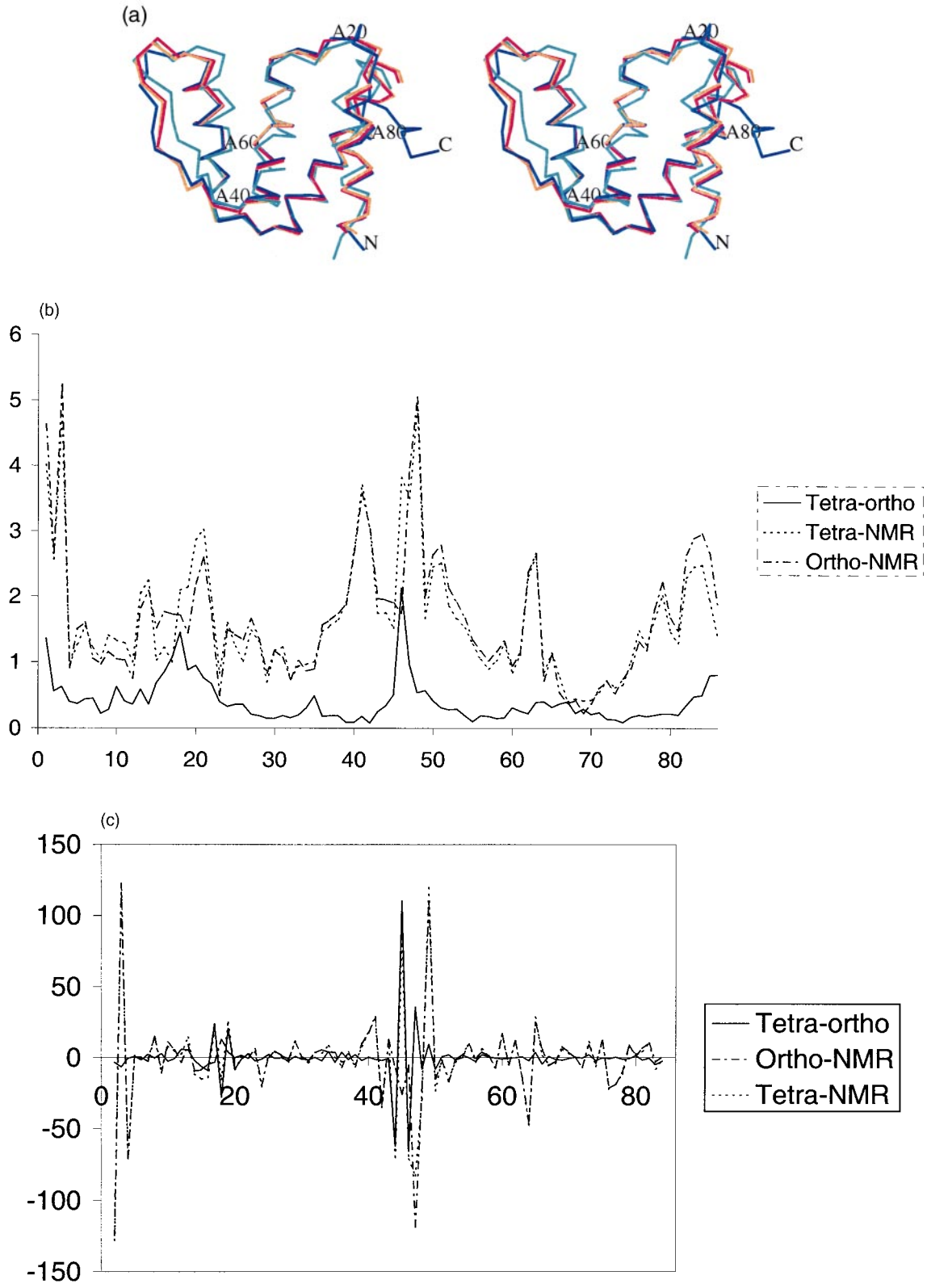

Figure 4. (a) Stereo C^{α} trace of ACBP structures. bACBP in the tetragonal crystal form is shown in red, bACBP in the orthorhombic crystal form in brown, the bACBP NMR structure in green and the PfACBP crystal structure is shown in blue. Every 20th residue in bACBP is labelled. (b) Comparison of the bACBP NMR and crystal structures. The distances between corresponding C^{α} atoms are shown for the tetragonal *versus* the orthorhombic crystal form as a continuous line, tetragonal form *versus* NMR as a dotted line, and orthorhombic form *versus* NMR as a broken line. (c) Comparison of C^{α} dihedral angles. The differences in dihedrals defined from C^{α} atoms are shown for the tetragonal *versus* the orthorhombic crystal form (continuous line), tetragonal form *versus* NMR (dotted line), and orthorhombic form *versus* NMR (broken line).

loops. The largest differences are found at the N-terminal region and the region around residues 46-47. These two regions are not well defined in the apo form NMR structures as there were only a few experimental restraints measured for these regions.[9]

The search for exploitable differences

Sequence alignment of PfACBP to the ACBP family (Figure 1) reveals a feature in PfACBP not found in any other ACBP in the sequence database. The loop between helices H1 and H2 (residues 14-22) is two residues longer and curls upwards towards the panthothenic acid moiety, reaching into the ligand binding pocket as previously defined by the bACBP NMR structure (Figure 5). After superposition of the NMR structures on the PfACBP crystal structures, there are significant steric clashes between this loop and the conformations of the ligand seen in the NMR structures (Figure 6). Although the conformation of the pantothenic acid moiety in the PfACBP crystal structure is not defined, it is likely that it is rather different from that in the bACBP structure. Interestingly, the bACBP NMR data show that several chemical shift values of residues in this area change significantly upon ligand binding, confirming intimate interaction of the ligand with this loop. Thus, it is possible that the longer loop in PfACBP may force the ligand in a conformation different from that seen in the bACBP structure.

Further analysis of the molecular surfaces revealed several other differences (Figure 5). The surface beneath the adenosine-3′-phosphate moiety is slightly more positively charged in PfACBP. In addition, there is a concentration of negative charge on the solvent exposed side of the long loop between helices H2 and H3 (residues 37-50). The most pronounced difference between PfACBP and bACBP can be observed near the end of the acyl chain. Whereas in bACBP a tunnel is observed allowing acyl chains longer than C_{16} to bind, the terminal carbon of the acyl chain in PfACBP sits in a pocket, suggesting that binding of longer-chain acyl-CoA molecules would be less favourable, which is in broad agreement with the binding assays described above. Superposition of the PfACBP crystal structure onto the bACBP-palmitoyl-CoA NMR structure shows that the C_{16} atom of palmitoyl-CoA in the bovine structure superimposes with the well-ordered (B-factor = 46.5 Å^2) terminal atom of the acyl chain in PfACBP (Figure 6). This suggests that the terminal acyl carbon is relatively immobile, leaving the pantothenic acid moiety and the first carbon atoms of the acyl chain to take on different conformations to adopt longer acyl chain lengths.

A detailed comparison of the residues lining the ligand-binding pocket is shown in Figure 6. It appears that most of the residues that hydrogen bond to the adenosine-3′-phosphate are conserved. All oxygen atoms of the 3′-phosphate moiety are involved in hydrogen bonding to residues that are completely conserved (Figure 1). In binding studies with an acyl-CoA derivative lacking this phosphate group, a 40 % reduction in binding energy was observed, indicating the importance of these interactions.[13] Analysis of amino acid differences in the ligand-binding pocket reveals a subset that may be responsible for the differences in acyl chain specificity described earlier, and also shows additional changes that could be exploitable (Figure 6). The Ala53Lys, Lys50Ile and Asp21Asn differences from bACBP to PfACBP are responsible for the closure of the tunnel at the terminus of the acyl chains, possibly limiting the chain length preference in PfACBP. The Val12Ile, Lys13Asn, Pro19Leu,

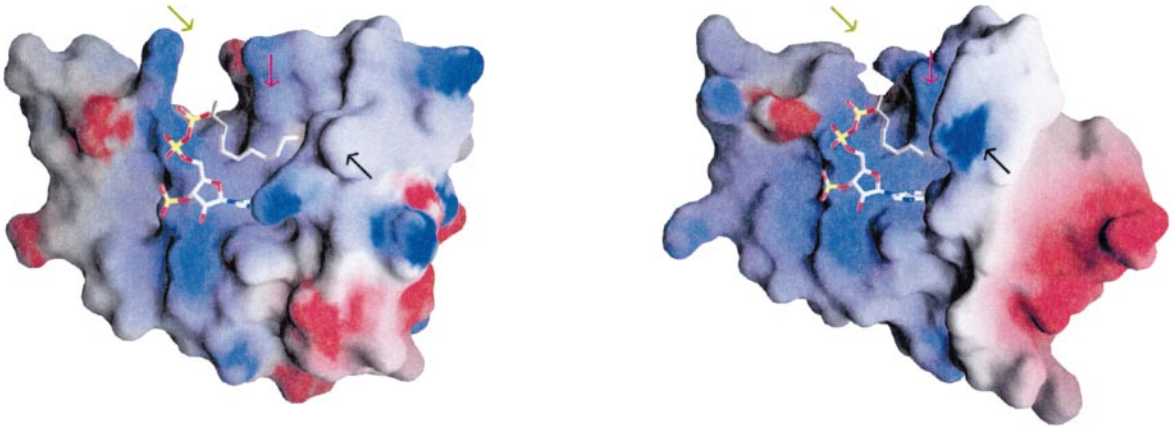

Figure 5. Comparison of PfACBP and bACBP electrostatic molecular surfaces. Molecular surfaces calculated from the (orthorhombic) bACBP (left) and PfACBP (right) crystal structures. The surfaces are coloured by GRASP electrostatic potential: red = − 6 kT, blue = + 6 kT. A stick representation of the PfACBP acyl-CoA ligand is shown. The ligand for bACBP was modelled by superposition of the PfACBP backbone and ligand onto the bACBP backbone. The three main differences are indicated by arrows: the insertion (see also Figure 1) in PfACBP (black arrows), the pocket near the end of the acyl chain (green arrows) and the Met24Lys change (purple arrows).

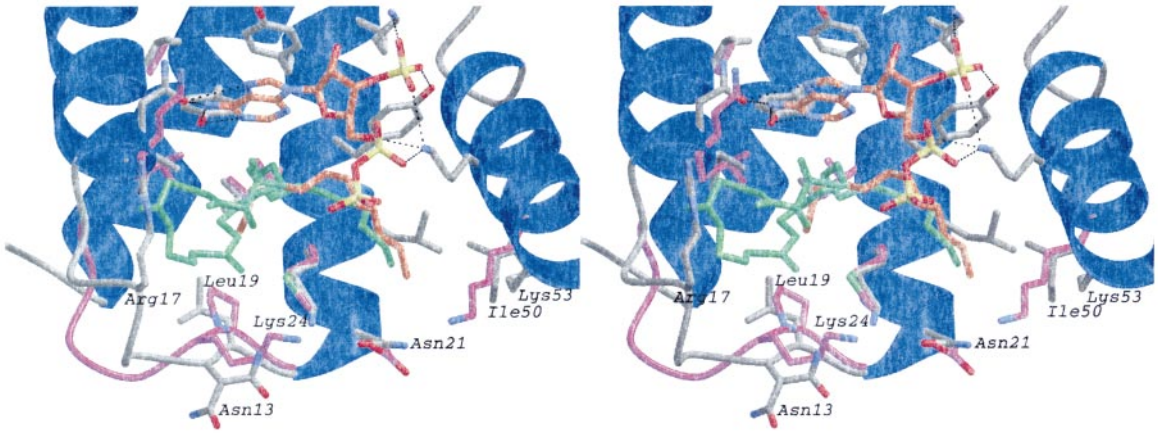

Figure 6. Stereo image of the superposed PfACBP and bACBP ligand-binding pockets. The PfACBP backbone is shown as a ribbon drawing. The shorter loop in bACBP between helices H1 and H2 is shown in magenta. PfACBP side-chains lining the ligand binding pocket are shown as sticks and coloured by atom type. bACBP side-chains that are different from PfACBP are shown as magenta sticks. Acyl-CoA in the PfACBP structure is shown as a stick model coloured by atom type, except for carbon atoms which are coloured orange. A green stick model of the pantothenic acid, cysteamine and acyl moieties of the pamitoyl-CoA ligand as seen in the bACBP NMR structure is also shown. Residues discussed in the text are labelled.

changes and Arg17 insertion (together with the loop backbone) change the interaction with the pantothenic acid moiety. The most significant single side-chain difference is Met24Lys. Alignment of all ACBP isoforms shows that, with the exception of PfACBP and testis-specific ACBPs,[3] only a large hydrophobic amino acid is allowed (methionine or leucine) at this position. The reason for general conservation of the methionine residue is revealed by the position of this residue with respect to the ligand (Figure 6). The acyl chain wraps around the β,γ and δ atoms of the side-chain. Analysis of the holo-bACBP NMR ensemble further shows that a subset of structures have a χ_3 methionine side-chain torsion angle of around 50°, bringing the C^{ε} atom close (around 3 Å) to the methylene groups on the acyl chain. In PfACBP $\chi_3 = -68°$ for the lysine residue, thus avoiding an unfavourable contact between the lysine N^{ζ} atom and the acyl chain (Figure 6).

Discussion

The cloning and characterization of *P. falciparum* ACBP has revealed a number of marked differences with its bovine homologue. PfACBP prefers acyl-CoAs with a significantly shorter chain length than bACBP. ACBP from *T. brucei* was recently characterized,[5] and its sequence shows a number of features similar to the PfACBP sequence described here, including the loop insertion, the Met24Lys change and the tighter pocket at the end of the terminus of the acyl chain (Figure 1). In that study it was shown that ACBP in *T. brucei* is the donor of myristoyl-CoA for fatty acid remodelling in GPI biosynthesis. This type of fatty acid remodelling reaction does not occur in human GPI biosynthesis and may thus represent a potential drug target. The fact that both *T. brucei* and *P. falciparum* have a slight preference for myristoyl-CoA, whereas the specificity for bACBP is narrower and centered around longer acyl chains, makes it tempting to speculate a similar role for both parasite proteins. However, even if PfACBP is not involved in GPI biosynthesis, it is still likely to be required for regulation of cell metabolism and signaling. This notion is supported by an ACBP gene knock-out mutant in yeast, which showed that the knock-out mutant was unable to compete with wild-type yeast, suggesting a perturbation of acyl-CoA metabolism.[14] Thus, provided exploitable differences between the mammalian and *P. falciparum* ACBPs can be found, rational drug design to selectively block the PfACBP acyl-CoA binding site could have an effect on normal parasite survival.

Comparison of the high-resolution bACBP and PfACBP crystal structures obtained in this study, together with the bACBP NMR structures, has revealed a number of differences between the two ACBPs. The possible structural basis for the slightly shorter acyl chain specificity of PfACBP may lie in the insertion in the loop between the H1 and H2 helices, and in the closure of the tunnel at the terminus of the acyl chain through three side-chain changes. This suggests that one level of selectivity may be achieved by using a short/medium-length acyl chain as a template for blocker design. An additional level of selectivity for PfACBP *versus* bACBP may be achieved by exploitation of two non-conservative changes: the inserted Arg17 pointing into the binding pocket towards the pantothenic acid moiety, and the non-conservative Met24Lys difference which introduces hydrogen bonding potential and a possible positive charge within contact distance of the acyl chain. Both differences could be exploited by introducing

hydrogen bonding acceptors and/or negative charges on a template molecule for selective blocking of the PfACBP binding site.

Materials and Methods

Cloning, expression, purification and characterization of *P. falciparum* ACBP

A genomic DNA clone of *P. falciparum* (accession number AA549985) was kindly provided by J. Dame (Department of Pathobiology, University of Florida). Routine DNA manipulations were performed in *E. coli* strain DH5α. All chemicals were of the highest grade available from BDH-Merck or Sigma and restriction enzymes were from Promega. DNA sequencing of double-stranded DNA was accomplished by the dideoxynucleotide chain termination method by automated cycle sequencing using the dye terminator method (ABI PRISM big dye terminator kit; Perkin Elmer).

A BLAST search of the *P. falciparum* genomic sequences in the TIGR database was performed using the gene encoding *T. brucei* ACBP which has been described recently.[5] An open reading frame (ORF) corresponding to the *P. falciparum* ACBP sequence was identified (accession number AA549985). The gene was obtained by polymerase chain reaction (PCR) amplification of the *P. falciparum* ORF from genomic DNA, using forward primer 5′-ggcatatggcacaagtatttg-3′ and reverse primer 5′-ggctcgagttattccccatcttg-3′. The forward primer contained an *Nde*I site and the reverse primer contains a *Xho*I site for cloning. Amplification conditions were 94 °C for 45 seconds, 50 °C for one minute and 72 °C for one minute for 30 cycles. The PCR product was blunt-end ligated into the *Sma*I site of pUC18 (Sureclone kit; Amersham Pharmacia Biotech) giving the plasmid pUC18-*Pf.ACBP*. The insert was excised by digestion with *Nde*I and *Xho*I and ligated into the *Nde*I and *Xho*I cloning site of the pET16b expression vector (Novagen). The pET16b-*Pf.ACBP* plasmid was transformed into competent BL21 (DE3) *E. coli* cells. A single colony was grown up in Luria-Bertani broth containing 0.1 mg/ml ampicillin. When the culture reached an A_{600} of 0.5 in a volume of one litre, 1 mM isopropyl-D-thiogalactopyranoside was added to induce expression of recombinant *P. falciparum* ACBP. Cultures were grown for an additional three hours at 37 °C and then harvested by centrifugation (4000 ***g***, ten minutes, 4 °C). Cells were resuspended in 100 ml of lysing buffer (20 mM Bis-Tris propane, 20 mM Tris-HCl pH 7.5, 300 mM NaCl, 1 mM phenylmethanesulfonyl fluoride, 2 μg/ml leupeptin, 0.2 mM *N*-tosyl-L-lysine chloromethylketone and 0.1 mg/ml lysozyme) for 15 minutes at 30 °C and disrupted by sonication (6 × 30 second pulses interrupted with cooling on ice). Cell debris was removed by centrifugation at 10,000 ***g*** for ten minutes prior to applying the supernatant to a Ni^{2+}-resin column (1.6 cm × 12 cm Chelating Sepharose Fast Flow; Amersham Pharmacia Biotechnology). The histidine-tagged recombinant protein was eluted from the column with a 10 mM to 1 M linear gradient of imidazole in 20 mM Bis-Tris propane, 20 mM Tris-HCl (pH 7.5), 300 mM NaCl at 3 ml/minute. Fractions were desalted and concentrated with a Centricon plus-20 (Amicon) filtration unit and treated with 50 μg factor Xa protease (New England Biolabs) per milligram recombinant protein for three days at 4 °C in digestion buffer (20 mM Tris-HCl (pH 8.0), 100 mM NaCl, 2 mM $CaCl_2$). The recombinant protein was further purified on a gel permeation column (1 cm × 30 cm Superdex 75 HR; Amersham Pharmacia Biotechnology) in 50 mM Na-Hepes (pH 7.5), 300 mM KCl at 0.5 ml/minute. The sample was concentrated to 20 mg/ml using a Centricon plus-20 and stored at 4 °C.

The acyl-CoA content of PfACBP purified from *E. coli* was characterized by high performance liquid chromatography (HPLC). A 100 μl sample of purified, PfACBP (15 mg/ml) was applied on an ODS 10/100 column (4.6 mm × 250 mm) equilibrated with 30 % solvent B (80 % acetonitrile in 20 mM KH_2PO_4, pH 5.3) in solvent A (20 % acetonitrile in 20 mM KH_2PO_4, pH 5.3), without any pretreatment. The CoA esters were eluted with the following gradient of solvent B in solvent A: 30 % B in A for 20 minutes, 30-40 % B in 30 minutes, 40-45 % B in ten minutes, 45-60 % B in 20 minutes, 60-85 % B in five minutes, and 85 % B for five minutes. The flow-rate was 1.0 ml/minute.

An acyl-CoA competition binding assay was performed as described.[15] Recombinant *P. falciparum* and bovine ACBP were stripped of bound acyl-CoAs using reverse phase HPLC.[16] Aliquots of 0.05 pmol ACBP in 25 μl binding buffer (10 mM potassium phosphate, pH 7.4) were mixed with 0.1 pmol of unlabelled acyl-CoA and 0.1 pmol [^{3}H]myristoyl-CoA in 75 μl of binding buffer. The samples were incubated at 37 °C for 30 minutes, chilled on ice for ten minutes and mixed with 0.2 ml of an ice-cold 50 % slurry of Lipidex 1000 (Canberra Packard) in binding buffer. After 100 minutes on ice, the samples were centrifuged at 12,000 ***g*** for five minutes at 0 °C. The radioactivity in 100 μl of the resulting supernatant was determined by scintillation counting. The assay was carried out in triplicate and controls without ACBP were performed.

An acyl-CoA binding specificity study was performed using isoelectric focusing analysis as described.[16] Aliquots of 5 μg ACBP were incubated with 0.5 μg of acyl-CoA (C10-20) in 10 μl of 10 mM potassium phosphate (pH 7.4) at 37 °C for ten minutes and resolved on Novex isoelectric focusing gels with ampholytes for the pH range 3-10.

Crystallization

Recombinant bovine ACBP (bACBP) was prepared and purified as described.[17] All crystallization trials were carried out using the hanging drop vapour diffusion method. Tetragonal bACBP crystals were obtained using a reservoir solution composed of 25 % polyethylene glycol 5000 monomethyl ether (PEG 5000 MME), 40 mM $Ni(SO_4)_2$, 40 mM Hepes buffer (pH 7.5). A drop containing 4 μl of reservoir and 4 μl of 18 mg/ml protein solution was equilibrated against 1 ml of the reservoir solution at 4 °C. Bi-pyramidal crystals appeared within one week reaching a full size of approximately 0.2 mm × 0.3 mm × 0.3 mm.

Orthorhombic bACBP crystals were obtained by mixing a 4 μl solution of 15 % PEG 8000, 5 mM $CdCl_2$, 10 mM Hepes buffer (pH 7.5) with 4 μl of 10 mg/ml bACBP complexed with palmitoyl-CoA at a 1:1 molar concentration ratio. The drops were equilibrated against 25 ml of 0.2 M NaCl at 20 °C. No crystals were observed during the first two months after the experiments were set up. One crystal with well-defined shape was eventually found after the drops were allowed to equilibrate for ten months. This crystal was used both for space group determination with precession photography and for intensity data collection.

PfACBP was crystallized using the hanging drop vapour diffusion method. Protein solution (2 μl) containing 15 mg/ml protein, 50 mM Hepes (pH 7.5) and 300 mM KCl was mixed with 2 μl of well solution (10 mM $NiCl_2$, 100 mM Tris (pH 8.5), 20 % PEG 2000 MME). Trays were stored at 20 °C, and crystals appeared after two to three days, reaching a maximum size of 0.05 mm × 0.05 mm × 0.3 mm.

Data collection

Precession photography of the orthorhombic bACBP crystal form showed that it belonged to $P2_12_12$ or $P2_12_12_1$. Intensity data were then collected to a resolution of 2.0 Å using a Hamlin/Xuong (UCSD-type) area detector mounted on a Rigaku rotating anode generator equipped with graphite monochromator. Software described by Howard *et al.*[18] was used for data collection and processing. The space group was determined to be $P2_12_12_1$ with unit cell dimensions $a = 26.1$ Å, $b = 54.8$ Å, and $c = 65.8$ Å. Details of data processing are given in Table 4.

Systematic absences obtained for the bi-pyramidal bACBP crystal form by precession photography showed it to be in a tetragonal space group. Diffraction datasets were collected to a resolution of 2.4 Å at room temperature using a Hamlin/Xuong (UCSD-type) area detector and an R-Axis IIc imaging plate detector mounted on a Rigaku rotating anode X-ray generator. The images were integrated and scaled using the programs from the *HKL* suite.[19] The space group was determined to be either $P4_1$ or $P4_3$ with cell parameters $a = b = 47.8$ Å and $c = 128.8$ Å. The two data sets were merged to give a complete data set to 2.4 Å resolution and used for molecular replacement calculations. At a later stage, a data set to a resolution of 2.0 Å was collected from a single crystal using a MAR image plate detector at the beamline X11 at the EMBL Outstation, DESY, Hamburg, and processed using the *HKL* suite[19] (Table 4).

Diffraction data for PfACBP were collected on beamline BW7A, EMBL Outstation, DESY, Hamburg, using a MAR CCD detector. The crystal was cryoprotected by adding 50 % 2-methane-2,4-pentanediol to the mother liquor for 60 seconds, after which the crystal was frozen in a nitrogen stream. Initial oscillation images indicated a tetragonal lattice with $a = b = 48.7$ Å, $c = 48.4$ Å. A full dataset was collected to 2.0 Å resolution and processed with the *HKL* suite[19] (Table 4). Analysis of the Matthew's coefficient indicated that only a space group with four symmetry operations was allowed, and the systematic absences along the 4-fold axis indicated a $P4_1$ or $P4_3$ space group.

Structure determination and refinement

All structures were solved by molecular replacement using AMoRe.[20] Model building was performed using O,[21] and refinement with CNS.[22] Quality of intermediate models was monitored using PROCHECK[23] and WHAT IF.[24]

The solution of the bACBP crystal structure has been briefly described.[25] For the bACBP orthorhombic crystal form, the search models were derived from the NMR models of bACBP complexed with palmitoyl-coenzyme A[10] (PDB entry 1ACA) , which were kindly provided by F.M. Poulsen (Carlsberg Laboratory, Denmark) before their general release from the PDB. A solution was found using an ensemble of the 14 most similar models from the family of 20 NMR structures[10] superimposed on top of each other as a search model. A solution was found with AMoRe with a CC of 0.441 (*R*-factor 0.525, next best solution had CC 0.437 and *R*-factor 0.540) within the resolution range 15-3.0 Å. The crystal packing of the best solution looked good and the maps calculated using phases from the model looked convincing for most of the protein. Despite rather high-resolution diffraction data collected for the orthorhombic crystal form, the refinement, which included simulated annealing, proved to be difficult due to the lack of independent phase information, and R_{free} stalled at 0.46 ($R = 0.36$). The partially refined model, however, was sufficiently improved to be used to solve the bACBP tetragonal crystal form (described below). Using this refined model, the orthorhombic crystal form could be refined further. By alternating SA refinement, manual rebuilding, and addition of solvent molecules, the model was refined with CNS[22] using the amplitude-based maximum likelihood function. All data between 20.0 and 2.0 Å resolution were used in the refinement and the bulk solvent correction implemented in CNS was applied, resulting in the final model (Table 2) with an *R*-factor of 0.200 ($R_{free} = 0.226$) (Figure 2(a)). A search for the palmitoyl-CoA ligand in the crystal was unsuccessful, as no electron density which could account for whole or part of the ligand was found. A possibility is that the ligand was hydrolysed during the relatively long period of crystallization.

Table 4. Details of data collection, processing and merging

	Ortho-bACBP	Tetra-bACBP	PfACBP
Temperature (K)	298	120	100
Wavelength (Å)	1.54	0.928	1.03
Space group	$P2_12_12_1$	$P4_1$	$P4_3$
Cell dimensions (Å)	$a = 26.1$, $b = 54.8$, $c = 65.8$	$a = b = 47.8$, $c = 128.8$	$a = b = 48.7$, $c = 48.4$
Resolution range (Å)	8-2.0(2.15-2.0)	40-2.0(2.07-2.0)	25-2.0(2.07-2.0)
No. observed refl.	24,078 (2567)	50,106 (5001)	28,439 (2526)
No. unique refl.	6473 (1196)	18831 (1917)	7754 (736)
Redundancy	3.7 (2.1)	2.7 (2.6)	3.7 (3.4)
$\langle I/\sigma I \rangle$	32.7 (9.3)	13.8 (3.6)	16.2 (2.7)
Completeness (%)	94.9(91.2)	96.5(98.8)	99.4(95.3)
R_{merge}	0.040(0.076)	0.066(0.292)	0.058(0.516)
NCS	None	3-fold	None
$V_{Matthews}$ (Å^3/Da)	2.4	2.5	2.6

Values in parentheses are for the highest resolution shell. Ortho-bACBP, bACBP orthorhombic crystal form; tetra-ACBP, tetragonal bACBP crystal form.

As described above, the partially refined structure for the bACBP orthorhombic crystal form was used as a search model for molecular replacement with the bACBP tetragonal form reflection data. After the rotation function, a translation function search was carried out in both $P4_1$ and $P4_3$, with the results being consistently better for the former. The best solution after rotation and translation function had a CC of 0.291 and *R*-factor of 0.517 (next best: CC 0.277, *R*-factor 0.526) for data between 15.0 and 4.0 Å resolution. These were improved after RBR to CC of 0.402 and *R*-factor of 0.525 in the resolution range 15.0-2.7 Å. Keeping this solution fixed, a second translation search was performed. A solution for the second molecule was found and combining these two solutions, the correlation coefficient improved to 0.498 (*R*-factor 0.490) after RBR. The search for a third molecule from these rotation peaks was unsuccessful. However, analysis of the crystal packing on a graphics display, revealed a well-defined void for a third molecule. Therefore another rotation search using data between 15.0 and 3.0 Å resolution was carried out. The 48th peak in the rotation function gave the best score in the combined translation function with AMoRe. After RBR using data between 15.0-2.7 Å resolution of all three molecules, the correlation coefficient was 0.587 and the *R*-factor was 0.451 (the next best solution had CC and *R*-factor of 0.522 and 0.487, respectively). The three molecules were related by 3-fold NCS along the *a*-axis. Several cycles of rebuilding and simulated annealing refinement with NCS produced a model with an R_{free} of 0.259 ($R = 0.207$) for data to 2.4 Å resolution. At this stage a 2.0 Å dataset was collected at the EMBL-Outstation, DESY, Hamburg (Table 4). Refinement was continued using CNS[22] with this high-resolution data, which involved mainly adjusting some side-chain conformations and inclusion of more solvent molecules. All data between 20.0 and 2.0 Å resolution were used in the refinement and the bulk solvent correction implemented in CNS was applied. The final model has an *R*-factor of 0.223 ($R_{free} = 0.255$) (Table 2; Figure 2(a)).

Initial attempts to solve the PfACBP structure using the NMR ensemble of bACBP structures as search models were unsuccessful. Using the tetragonal bACBP crystal structure, a solution was found ($R = 0.463$, $CC = 0.313$ after RBR) in $P4_3$, with a poly-alanine backbone model plus side-chains conserved between bACBP and PfACBP. An initial map revealed good density for most of the backbone and it was possible to identify most of the new side-chains. Since good quality diffraction data were collected (Table 4), this initial set of phases was used as input for the autobuilding procedure with warpNtrace.[26] Standard protocols were used, with a relatively large number (1000) of cycles of rebuilding and refinement. A total of 75 out of the 90 residues were automatically built, including their side-chains. After an initial round of model building in O[21] and refinement in CNS[22] the maps revealed interpretable density for the missing pieces of backbone and side-chains ($R = 0.295$, $R_{free} = 0.344$). After the next macrocycle, which included simulated annealing, well-defined density in the binding site (Figure 2(b)) could be observed for the nucleotide moiety of CoA, which was included ($R = 0.267$, $R_{free} = 0.312$). The new maps revealed two strong peaks close to His0 and His49, and density for a fatty acid (Figure 2(b)). Using the phases of the model and the anomalous differences from the reflection data set, a map was calculated that showed the same two peaks (>4σ). The peaks were interpreted as coordinated Ni^{2+}, which were the only heavy atoms present in the crystallization solution. A string of 13 carbon atoms was modelled in the density for the acyl chain ($R = 0.206$, $R_{free} = 0.255$). Further inclusion of solvent molecules, two sulphate ions and some alternate side-chain conformations resulted in the final model ($R = 0.198$, $R_{free} = 0.237$) (Table 4).

PDB accession codes

The coordinates and structure factors have been deposited in the RCSB data bank with accession codes 1HBK, 1HB6, and 1HB8.

Acknowledgements

We thank the EMBL-Hamburg outstation for use of beamlines BW7A and X11 at DESY, and Flemming Poulsen for access to the coordinates of the bACBP NMR structure prior to their public release. K.G.M. is a Beit Memorial Fellow, D.v.A. is supported by a Wellcome Trust Career Development Research Fellowship.

References

1. Brockman, A., Price, R. N., van Vught, M., Heppner, D. G., Walsh, D., Sookto, P., Wimomwattrawatee, T., Looareesuwam, S., White, N. J. & Nosten, F. (2000). Plasmodium falciparum antimalarial drug susceptibility on the north-western border of Thailand during five years of etensive use of artesunate-mefloquine. *Trans. Roy. Soc. Trop. Med. Hygiene,* **94**, 537-544.
2. Faergeman, N. J. & Knudsen, J. (1997). Role of long-chain fatty acyl-coA esters in the regulation of metabolism and in cell signalling. *Biochem. J.* **323**, 1-12.
3. Kragelund, B. B., Knudsen, J. & Poulsen, F. M. (1999). Acyl-coenzyme a binding protein (ACBP). *Biochim. Biophys. Acta,* **1441**, 150-161.
4. van Aalten, D. M. F., DiRusso, C. C., Knudsen, J. & Wierenga, R. K. (2000). Crystal structure of FadR, a fatty acid-responsive transcription factor with a novel acyl coenzyme A-binding fold. *EMBO J.* **19**, 5167-5177.
5. Milne, K. G. & Ferguson, M. A. J. (2000). Cloning, expression and characterisation of the acyl-coA binding protein in African trypanosomes. *J. Biol. Chem.* **275**, 12503-12508.
6. Masterson, W. I., Raper, J., Doering, T. L., Hart, G. W. & Englund, P. T. (1990). Fatty acid remodeling: a novel reaction sequence in the biosynthesis of trypanosome glycosyl phosphatidylinositol membrane anchors. *Cell,* **62**, 73-80.
7. Kragelund, B. B., Poulsen, K., Andersen, K. V., Baldursson, T., Kroel, J. B., Neergard, T. B., Jepsen, J., Roepstoff, P., Kristiansen, K., Poulsen, F. M. & Knudsen, J. (1999). Conserved residues and their role in the structure, function and stability of acyl-coenzyme A binding protein. *Biochemistry,* **38**, 2386-2394.
8. Kragelund, B. B., Osmark, P., Neergaard, T. B., Schioedt, J., Kristiansen, K., Knudsen, J. & Poulsen, F. M. (1999). The formation of a native-like structure containing eight conserved hydrophobic residues is rate limiting in two-state protein folding of ACBP. *Nature Struct. Biol.* **6**, 594-601.

9. Andersen, K. V. & Poulsen, F. M. (1992). Three-dimensional structure in solution of acyl-coenzyme-A binding-protein from bovine liver. *J. Mol. Biol.* **226**, 1131-1141.
10. Kragelund, B. B., Andersen, K. V., Madsen, J. C., Knudsen, J. & Poulsen, F. M. (1993). Three-dimensional structure of the complex between acyl-coenzyme A binding protein and palmitoyl-coenzyme A. *J. Mol. Biol.* **230**, 1260-1277.
11. Kleywegt, G. J. & Jones, T. A. (1996). Phi/psi-chology: Ramachandran revisited. *Structure,* **4**, 1395-1400.
12. Korn, A. P. & Rose, D. R. (1994). Torsion angle differences as a means of pinpointing local polypeptide-chain trajectory changes for identical proteins in different conformational states. *Protein Eng.* **7**, 961-967.
13. Faergeman, N. J., Sigurskjold, B. W., Kragelund, B. B., Andersen, K. V. & Knudsen, J. (1996). Thermodynamics of ligand binding to acyl-coenzyme A binding protein studied by titration calorimetry. *Biochemistry,* **35**, 14118-14126.
14. Schjeling, C. K., Hummel, R., Hansen, J. K., Boersting, C., Mikkelsen, J. M., Kristiansen, K. & Knudsen, J. (1996). Disruption of the gene encoding the acyl-coA-binding protein (*acb1*) perturbs acyl-coA metabolism in *Saccharomyces cerevisiae*. *J. Biol. Chem.* **271**, 22514-22521.
15. Rosendal, J., Ertberg, P. & Knudsen, J. (1993). Characterisation of ligand binding to acyl-coA binding protein. *Biochem. J.* **290**, 321-326.
16. Knudsen, J., Faergeman, N. J., Skott, J., Hummel, R., Borsting, C., Rose, T. M., Andersen, J. S., Hojrup, P., Roepstorff, P. & Kristiansen, K. (1994). Yeast acyl-coA binding protein: acyl-coA binding affinity and effect on intracellular acyl-coA pool-size. *Biochem. J.* **302**, 479-485.
17. Mandrup, S., Hojrup, P., Kristiansen, K. & Knudsen, J. (1991). Gene synthesis, expression in *E. coli*, purification and characterization of the recombinant bovine acyl-coA binding protein. *Biochem. J.* **276**, 817-823.
18. Howard, A. J., Nielsen, C. & Xuong, N. H. (1985). Software for a diffractometer with multiwire area detector. *Methods Enzymol.* **114**, 452-472.
19. Otwinowski, Z. & Minor, W. (1997). Processing of X-ray diffraction data collected in oscillation mode. *Methods Enzymol.* **276**, 307-326.
20. Navaza, J. (1994). AMoRe: an automated package for molecular replacement. *Acta Crystallog. sect. A,* **50**, 157-163.
21. Jones, T. A., Zou, J. Y., Cowan, S. W. & Kjeldgaard, M. (1991). Improved methods for building protein models in electron density maps and the location of errors in these models. *Acta Crystallog. sect. A,* **47**, 110-119.
22. Brunger, A. T., Adams, P. D., Clore, G. M., Gros, P., Grosse-Kunstleve, R. W., Jiang, J.-S., Kuszewski, J., Nilges, M., Pannu, N. S., Read, R. J., Rice, L. M., Simonson, T. & Warren, G. L. (1998). Crystallography and NMR system: a new software system for macromolecular structure determination. *Acta Crystallog. sect. D,* **54**, 905-921.
23. Laskowski, R. A., McArthur, M. W., Moss, D. S. & Thornton, J. M. (1993). PROCHECK: a program to check the stereochemical quality of protein structures. *J. Appl. Crystallog.* **26**, 283-291.
24. Vriend, G. (1990). WHAT IF: a molecular modeling and drug design program. *J. Mol. Graph.* **8**, 52-56.
25. Kleywegt, G. J. (1996). Use of non-crystallographic symmetry in protein structure refinement. *Acta Crystallog. sect. D,* **52**, 842-857.
26. Perrakis, A., Morris, R. & Lamzin, V. S. (1999). Automated protein model building combined with iterative structure refinement. *Nature Struct. Biol.* **6**, 458-463.
27. Engh, R. A. & Huber, R. (1991). Accurate bond and angle parameters for X-ray protein-structure refinement. *Acta Crystallog. sect. A,* **47**, 392-400.

Edited by R. Huber

(Received 2 November 2000; received in revised form 19 March 2001; accepted 19 March 2001)